Cobalt Nanosized Particles Organized in a 2D Superlattice: Synthesis, Characterization, and Magnetic Properties

C. Petit,[†,‡] A.Taleb,[†] and M. P. Pileni*[,†,‡]

Laboratoire SRSI, URA CNRS 1662, Universite P. et M. Curie Bât F, 4 Place Jussieu, 75005 Paris, France, and CEA-Saclay, DSM-DRECAM Service de Chimie Moléculaire, 91 191 Gif sur Yvette Cedex, France

Received: June 24, 1998; In Final Form: September 9, 1998

Colloidal assemblies are used to synthesize FCC cobalt nanoparticles. The particles are coated, extracted from micelles, and characterized by transmission electron microscopy, small angle X-ray scattering, and electron and X-ray diffraction spectroscopy. These cobalt metal particles are stable in air, have a narrow size distribution, and on deposition on a graphite support, spontaneously form a 2D hexagonal network. The magnetic properties are compared when they are dispersed in a solvent and organized in 2D superlattices. Changes in the hysteresis loop and in the blocking temperature are observed and attributed to collective flip of the magnetization of adjacent particles.

I. Introduction

The synthesis of nanoparticles, characterized by a low size distribution, is a new challenge in solid state chemistry. Due to their small size, nanoparticles exhibit novel material properties that differ considerably from those of the bulk solid state.[1] Since the early 1980s, chemists and physicists have tried to obtain materials in a nanometer scale and have succeeded in drastically reducing the characteristic size of inorganic particles.[2,3] Many reports on the quantum size effect in the photochemistry of semiconductors[4] or the emergence of metallic properties[5] with the size of the particles have appeared in the past few years. In this emerging field, finely divided magnetic nanoparticles are desirable due to their large domains of applications, especially for data storage devices and sensors. Although there has been a great deal of work on large magnetic nanoparticles,[6] and the magnetic properties of isolated atoms are well understood, there are many unanswered questions concerning the development of magnetic order on a macroscopic scale.[7,8] Hence magnetic clusters provide a link between the microscopic atomic level and the macroscopic state, which can contribute to understanding magnetism in both regimes. The goal is the creation of perfect nanometer-scale magnetic crystallites identically replicated with a long range order in a state that can be manipulated and understood as pure macromolecular substances. This is an ultimate challenge in present materials research and could help us to understand the basis of ferromagnetism. To develop this application, it is crucial to control the spatial arrangement of these nanoparticles in 2D or 3D arrays.

Colloidal chemistry is particularly well suited to synthesize nanoparticles.[2,9] However, there has been little work on magnetic nanoparticles obtained by this method[10−14] as, more commonly, technically difficult methods such as chemical vapor deposition or molecular beams are used.[7,8] This is especially the case for metallic clusters. These metallic particles are not stable outside the molecular beam chamber due to oxidation processes and aggregation.[7]

Recently, it has been shown that synthesis in reverse micelles combined with precipitation can lead to highly monodispersed metal[15] or semiconducting nanoparticles[16] that spontaneously form 2D or 3D networks. Usually, in the case of magnetic particles such networks are only obtained by the lithographic method and the particle size is about 50 nm.[17] More recently, some organization of cobalt nanoparticles embedded in aluminum were reported in a magnetic multilayer obtained by cathodic sputtering.[18] Wang et al. report the formation of self-assembling tetrahedral cobalt oxide nanocrystals.[19] However, in this case the particles are obtained by decomposition of organometallic compounds and coated by AOT after synthesis to prevent aggregation. A mixture of cobalt oxide and cobalt is formed, and it is necessary to separate these two populations.[20] No attempt was made to study the magnetic properties.

Here, we report the magnetic response of these self-assembled 2D monolayers of cobalt nanosized particles. A comparison is made between the magnetic properties of cobalt nanoparticles in the self-assembled state and isolated in solution.

II. Experimental Section

1. Products. All materials were used without further purification. $CoCl_2$, AOT, and sodium borohydride, $NaBH_4$, were purchased from Sigma; isooctane was from Fluka. The synthesis of $Co(AOT)_2$ has been described elsewhere.[5a] $Co(AOT)_2$ is used as a stock solution at 0.125 M in isooctane.

2. Apparatus. Transmission electron microscopy (TEM) images and electron diffraction spectroscopy (EDS) patterns were obtained with a JEOL JEM 2000FX microscope. The solution was placed on a carbon-coated copper grid and evaporated under a nitrogen atmosphere. X-ray diffraction measurements (XRD) were carried out using a STOE Stadi P goniometer with a Siemens Kristalloflex X-ray generator with a cobalt anticathode ($\lambda = 1.7809$ Å) driven by a personal computer through a DACO-MP Interface. Atomic absorption spectroscopy, AAS, is done with a Perkin-Elmer PE 2380. The magnetic studies were performed using a commercial SQUID magnetometer Cryogenic S600.

3. Small Angle X-ray Treatment.[21] The scattered intensity $I(q)$ is the product of the form factor $P(q)$ and the structure factor $S(q)$, where q, the wave vector, is $4\pi \sin \theta/\lambda$ (2θ is the diffraction angle). The form factor gives the shape of the aggregates, and the structure factor takes into account interac-

[†] Universite P. et M. Curie.
[‡] DSM-DRECAM Service de Chimie Moléculaire.

10.1021/jp982755m CCC: $18.00
Published on Web 02/24/1999

tions between the aggregates. The particles volume fraction is calculated knowing the average amount of cobalt in solution as determined by atomic absorption spectroscopy (1 g/L), which gives a particle volume fraction, Φ_{pol}, of 0.01%. At such low particle volume fractions, aggregate interactions can be neglected and $S(q)$ is assumed to be 1.

For a homogeneous sphere with a sharp interface, the scattering intensity is given by

$$I(q) \approx P(q) = \Phi_{pol} V F \Delta\rho^2 [B(qR)]^2$$

with

$$B(x) = [3\{\sin(x) - (x)\cos(x)\}/(x)^3]$$

where R, V, F, and $\Delta\rho$ are the radius and volume of one particle, Thompson's factor (square of the classical electron radius, $F = 7.9 \times 10^{-26}$ cm^2),[21b] and the variation of the difference in the electron densities of the sphere and the surrounding medium, ρ_e and ρ_m, respectively. A convenient representation for homogeneous diffusing spheres is the Porod Plot, $I(q)\, q^4$ vs q, which emphasizes the scattering at large q and then focuses on the interface as[22]

$$\lim_{q\to\infty} I(q)\, q^4 = 2\pi(\Delta\rho)^2 S$$

where S is the total interfacial area. On assuming spherical particles having a shell structure with an internal and external core, the scattering intensity is given by

$$I(q) \approx P(q) = \Phi_{pol} V F\{(\rho_m - \rho_e)B(qr_e) + (\rho_e - \rho_i)B(qr_i)\}^2$$

where ρ_e and ρ_i are the electron densities of the external and internal core of the particle, respectively. The particle radius is given by

$$r = r_e + r_i$$

where r_i is the internal radius of the particles and r_e is the thickness of the shell.

The characteristic diameter of the particles D_c is related to the first maximum and minimum of this representation by D_c (nm) $= 0.54/q_{max} = 0.9/q_{min}$.

III. Results

1. Synthesis and Characterization. Reverse micelles are water in oil droplets stabilized by a monolayer of surfactant (e.g., sodium bis(2-ethylhexyl)sulfosuccinate, usually called Na(AOT)). The diameter of the droplets is controlled by the volume of solubilized water and varies from 0.5 to 18 nm. In this liquid solution, due to the Brownian motion, collisions between droplets induces exchange between water pools.[2] Hence, reverse micelles are defined as a microreactor and this property is used to produce cobalt particles.[11] A micellar solution of 0.25 M Na(AOT) and 2×10^{-2} M Co(AOT)$_2$ (cobalt bis(2-ethylhexyl)sulfosuccinate) is mixed with 0.25 M Na(AOT) micelles containing 2×10^{-2} M sodium tetrahydroboride, $NaBH_4$, as reducing agent. The two micellar solutions keep the same water content, i.e., the same diameter ($w = 10$, $d = 3$ nm). The synthesis is carried out in the presence of air. Immediately after mixing, the micellar solution remains optically clear and its color turns from pink to black, indicating the formation of colloidal particles. They are extracted from reverse micelles under anaerobic conditions, by covalent attachment of trioctylphosphine[23] and then redispersed in pyridine. This chemical surface treatment highly improves the stability of cobalt exposed to air. Thus cobalt nanoparticles could be stored without aggregation or oxidation for at least 1 week.

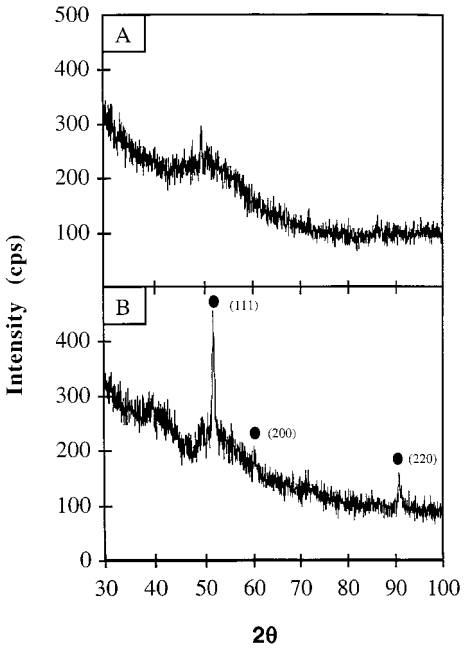

Figure 1. X-ray powder diffraction data on powders obtained after total evaporation of the solvent: (A) fresh powder isolated under inert conditions; (B) same sample after processing at 500 °C under nitrogen. The symbols correspond to the referenced data for FCC cobalt (JCPDS 15-806).

The composition of the extracted particles dispersed in pyridine, determined by atomic absorption spectroscopy, is 950 ± 50 mg/L of cobalt and 350 ± 25 mg/L of boron. The ratio B/Co is 37%.

Electron diffraction spectroscopy, EDS, shows large rings at 2 and 1.3 Å, as reported for Co metal particles.[24] No rings at 2.5 Å, characteristic of cobalt boride, Co_2B, are observed. After evaporation of pyridine under nitrogen, the X-ray powder diffraction (XRD) shows a large band centered at $\theta = 51.9°$ (i.e., $d = 2.03$ Å) (Figure 1A). However, the spectrum is poorly resolved and formation of cobalt boride ($\theta = 53.9°$, $d = 1.97$ Å) cannot be excluded. After the powder is annealed under N_2 at 500 °C for 2 h, the XRD spectrum shows the characteristic pattern of FCC cobalt metal[24] (Figure 1B). This is in good agreement with the structure of cobalt metal nanoparticles obtained elsewhere.[14] This differs from the bulk phase, which has an HCP structure.

The small angle scattered intensity $I(q)$ of particles dispersed in pyridine as a function of the wave vector q is recorded. To differentiate between particles having a sharp interface or a shell structure, various adjustments of the Porod plot are compared to experimental data (Figure 2). With a sharp interface, the electronic density profile is square (insert Figure 2A). With a shell structure, the composition of the internal and external core has to be defined. In all cases, cobalt metal is taken as one component and a boron derivative is selected for the second component. To determine the compound, we take into account the products usually formed in homogeneous solution. Hence, the shell structure consists of cobalt metal and either B_2O_3 or Co_2B. Borane, B_2H_6, is not selected as a second component because of its ability to form complexes with pyridine and phosphine.[29] We consider the following shell structures: (i) the internal core is cobalt metal surrounded either by B_2O_3 or by Co_2B with an electronic density profile shown in the Figure

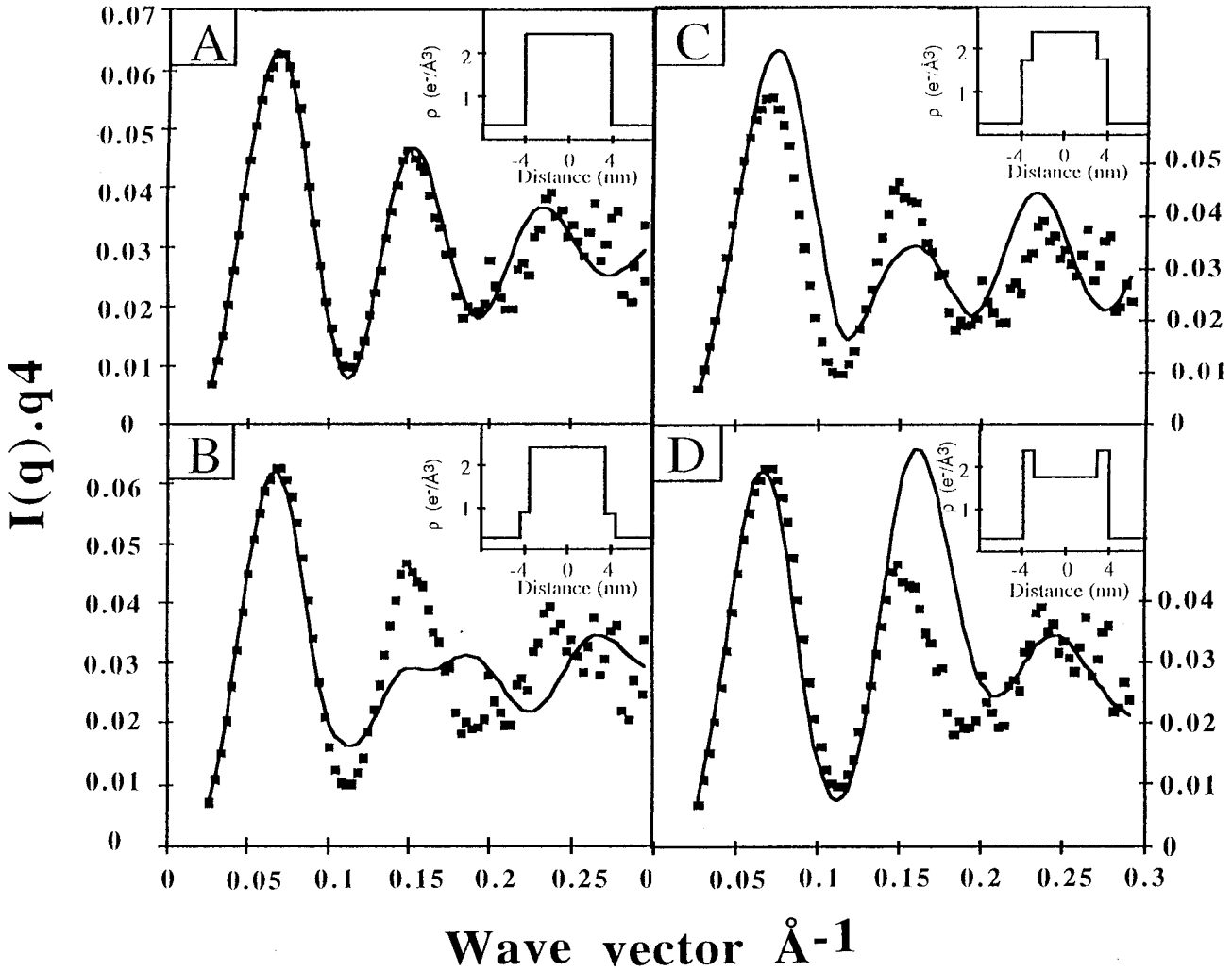

Figure 2. Small angle X-ray scattering data for cobalt nanosized particles after redispersion in pyridine (Porod's representation). The points represent the experimental data. The solid line is the best adjustment assuming a sphere with Gaussian polydispersity. Insets: the electronic density profiles used for the simulation. Key: (A) homogeneous particles of cobalt; (B) particles of cobalt (6 nm) surrounded by a shell of B_2O_3; (C) particles of cobalt (6 nm) surrounded by a shell of cobalt boride; (D) particles of cobalt boride (6 nm) surrounded by a shell of cobalt.

2B,C insets, respectively; (ii) the internal core is made of Co_2B with an external shell of cobalt metal, and the electronic profile is shown in the Figure 2D insert.

The electronic densities of pure metallic cobalt, ρ_{Co}, pyridine, ρ_{pyr}, trioctylphosphine, ρ_{top}, cobalt boride, ρ_{Co_2B}, and borate, $\rho_{B_2O_3}$, are 2.43, 0.31, 0.29, 1.77, and 0.8 $e^-/Å^3$, respectively. Because the values of ρ_{pyr} and ρ_{top} are very close, it is impossible to discriminate between these two values and the electronic density of the surrounded medium of the spherical particles, ρ_m, is taken equal to ρ_{pyr}.

Assuming particles are made of cobalt metal particles coated with trioctylphosphine and dispersed in pyridine, because ρ_{top} and ρ_{pyr} are very close, the interface is sharp. A good correlation between the experimental data and the simulated curve is obtained for 8 nm spherical particles with 9% as the size distribution (Table 1 and Figure 2A). It has to be noticed that the simulated and experimental data are in good agreement over a large q range, especially for the positions of the maxima and minima and their relative intensities.

The Porod plots corresponding to the various compositions that are obtained assuming a shell structure are shown in Figure 2B−D. When cobalt particles are coated by B_2O_3 (Figure 2B) a rather good adjustment is obtained for the first peak and no correlation between experimental data and simulation is observed for the large q value. By replacing B_2O_3 by Co_2B a better adjustment is obtained for the large angle (Figure 2C). However, the relative intensity of the peaks does not adjust the experimental data. Similar comments can be made for Co_2B coated by cobalt metal (Figure 2D). From these data it is reasonable to conclude that homogeneous cobalt spheres with a sharp interface are formed.

TABLE 1: Size of Cobalt Nanoparticles as Obtained by TEM and SAXS

experiments	diameter (nm)	polydispersity
TEM	5.8 ± 0.5	11%
SAXS (porod plot)	7.9 ± 0.5	
SAXS (simulation)	8 ± 0.25	9%

A drop of the solution is deposited on a carbon grid. Figure 3 shows TEM patterns obtained at various magnifications. The TEM grid is totally covered by particles that are arranged in a hexagonal network. The particle average size deduced from the histogram (Figure 3) is 5.8 nm diameter with a polydispersity of 11% (Table 2). No traces of shells are observed on the surface.

c. Magnetic Properties. Magnetic properties of the cobalt nanoparticles dispersed in pyridine and arranged in two dimensions on a carbon substrate are derived from zero field cooled and field cooled (ZFC/FC) curves and from magnetization curves at 3 K.

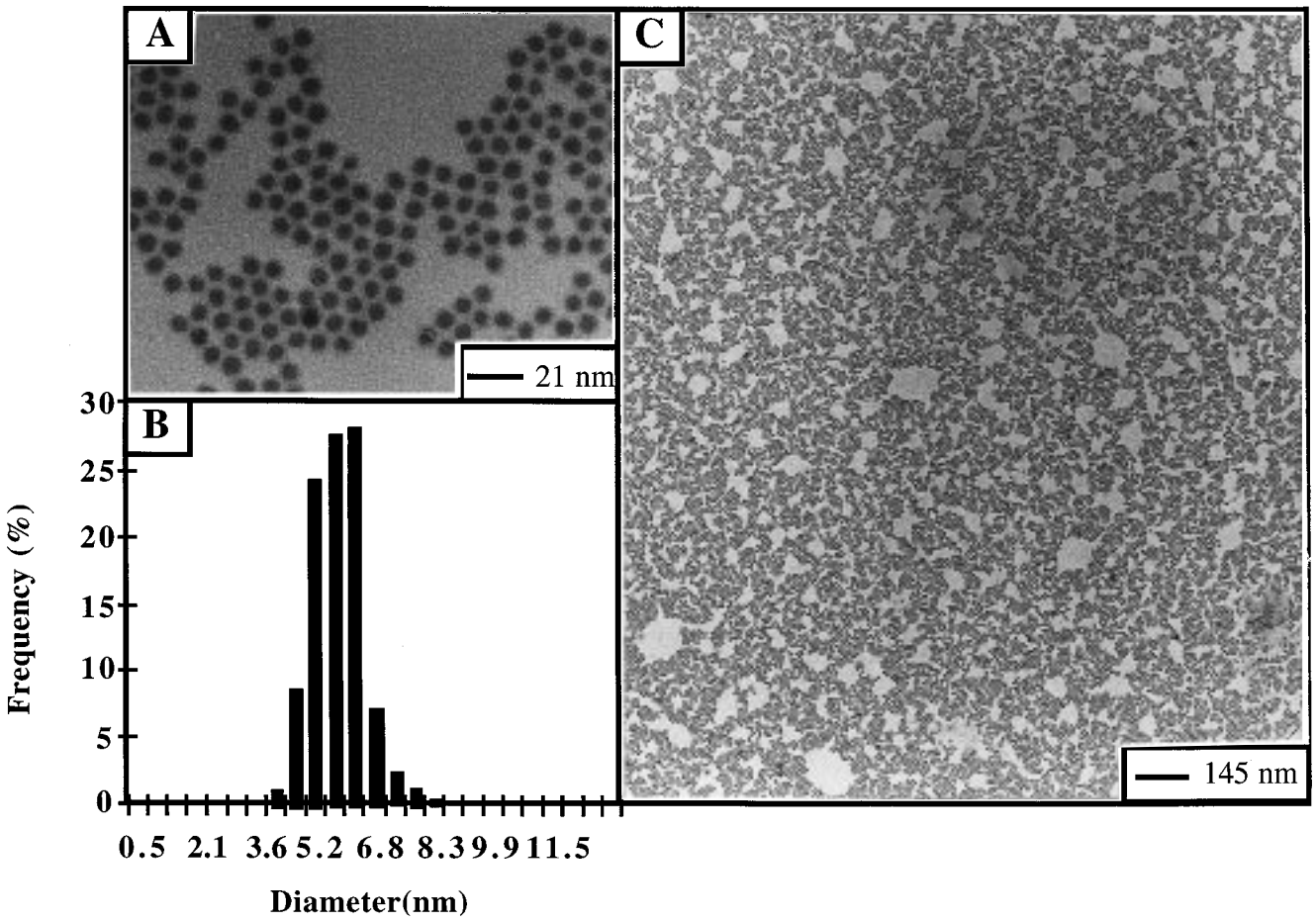

Figure 3. TEM patterns at different magnifications (A and B) and histogram of the size of the hexagonal ordered monolayer of cobalt nanoparticles. This spontaneous self-assembling is obtained by depositing a drop of solution on a TEM grid coated by amorphous carbon.

TABLE 2: Magnetic Properties of Cobalt Nanoparticles Isolated in Liquid and Organized on Graphite[a]

physical state	M_s (emu/g)	H_s (T)	M_r (emu/g)	M_r/M_s	H_c (T)
isolated in pyridine	80 ± 5	>2	20 ± 2	0.25	0.15
self-assembled on graphite	80 ± 5	1.5	35 ± 3	0.44	0.15

[a] H_s field at saturation, M_s magnetization at saturation, M_r remanent magnetization, H_c coercitive field.

The ZFC/FC curves are recorded with a 75 Oe field (Figure 4). The field cooled (FC) curves show a uniform decay and reach the zero field cooled (2FC) curve close to the peak. This confirms the superparamagnetic behavior at high temperature. Figure 4A shows ZFC/FC curves of cobalt nanoparticles dispersed in pyridine with a blocking temperature at 58 K. Using the average particle volume determined by TEM, the anisotropy constant is 2.4×10^6 erg/cm^3. This is in good agreement with the anisotropy constant reported for bulk FCC cobalt (2.7×10^6 erg/cm^3).[14] The ZFC/FC curve of particles deposited on a support with formation of the 2D hexagonal network is very similar to that observed with isolated particles (Figure 4B). However, the blocking temperature is reached at 63 K. This increase in the blocking temperature when the particles are arranged in a 2D network (63 K) compared to isolated particles (58 K) is attributed to interparticle interactions.

Below T_b, at 3 K, the particles are ferromagnetic. Figure 5A shows the hysteresis loop of Co nanoparticles dispersed in pyridine. At 2 T the magnetization is not totally saturated. The saturation magnetization, M_s, is estimated by zero extrapolation

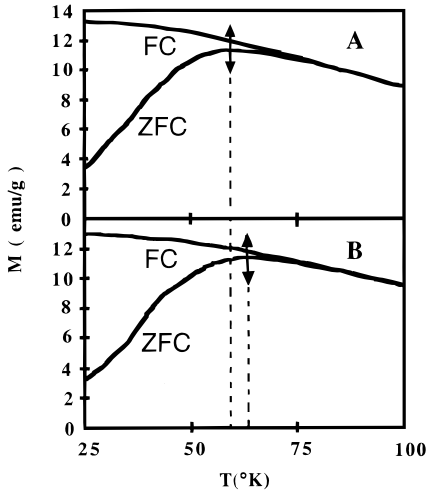

Figure 4. (A) ZFC/FC curve of a liquid solution of cobalt nanoparticles in pyridine. The peak indicates the transition between the ferromagnetic state (irreversible magnetization) and the superparamagnetic state (reversible magnetization with temperature). (B) ZFC/FC curve for cobalt nanoparticles deposited on cleaved graphite and dried under argon to prevent oxidation.

of the plot of magnetization versus $1/H$. $M_s = 80$ emu/g. This value is low compared to that obtained for the bulk phase (162 emu/g). Figure 5B shows the hysteresis loop of Co nanoparticles deposited on a graphite substrate. There is a clear change in the shape of the hysteresis loop. The magnetization is reached at 1.5 T and the ratio M_r/M_s markedly increases from 0.25 to 0.45 in comparison to isolated nanoparticles.

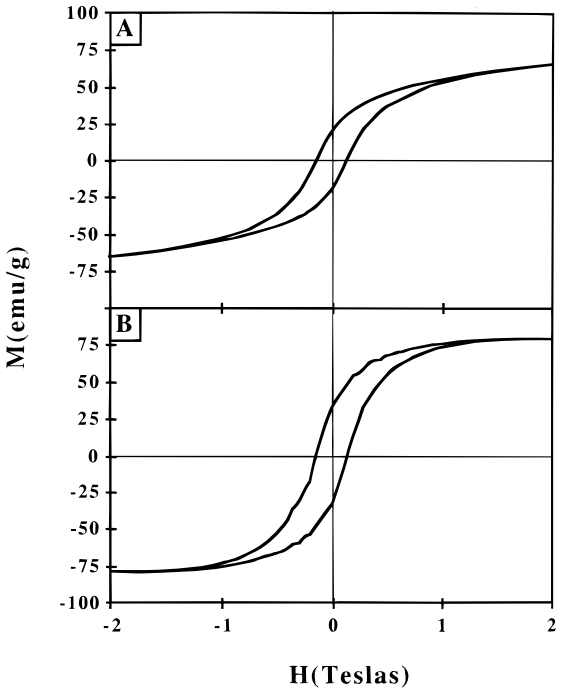

Figure 5. Hysteresis loop obtained at 3 K; (A) liquid solution of cobalt nanoparticles in pyridine; (B) cobalt nanoparticles deposited on cleaved graphite and dried under argon to prevent oxidation.

IV. Discussion

The reduction of transition metal ions by BH_4^- is a ubiquitous reaction that is useful for the production of ultrafine particles of metals and metal borides. Unfortunately, borohydride reduction chemistry is quite complex and the nature of the products strongly depends on the reaction conditions.[25,26] As an example, Klabunde et al. show that rapid mixing of cobalt ions and borohydrides yields metal particles under aerobic conditions with B_2O_3 as an underproduct of the reaction and cobalt borides under anaerobic conditions.[26] Furthermore, the solvent used to make the particles plays an important role in formation of the final product. In fact, the mechanism differs markedly in aqueous and in nonaqueous solution.

In aqueous solution, black precipitates of metal boride particles are formed as follows:[25]

$$2Co^{2+} + 4BH_4^- + 9H_2O \rightarrow Co_2B + 12.5H_2 + 3B(OH)_3 \quad (1)$$

In the presence of a relatively low amount of oxygen, Co_2B is reduced and cobalt metal is formed as follows:

$$4Co_2B + 3\,O_2 \rightarrow 8Co + 2B_2O_3 \quad (2)$$

An excess of oxygen oxidizes cobalt metal to its oxide derivative.

In nonaqueous solution cobalt metal particles are formed.[27] This has been explained by the fact that the nonaqueous solvent acts as a ligand, L, as follows:

$$Co^{2+} + 2NaBH_4 + nL \rightarrow (L)_nCo(BH_4)_2 + 2Na^+ \quad (3)$$

$$(L)_nCo(BH_4)_2 \rightarrow Co + H_2 + B_2H_6 + nL \quad (4)$$

Reverse micelles contain a water pool and the majority of the nonpolar solvent. Furthermore, it has been demonstrated that the water structure in the pool differs from the bulk phase[28] and we could expect that reverse micelles act as a nonaqueous solvent. However, the atomic absorption spectroscopy data obtained from coated particles do not demonstrate formation of metal cobalt particles. Conversely, it shows a high boron concentration (350 mg/L, i.e., a ratio B/Co of 37 wt %) in the solution made of coated particles dispersed in pyridine. Such a high boron concentration is inconsistent with formation of cobalt metal or cobalt boride particles in which the B/Co ratio is expected to be 0% whereas it is 8.2% for Co_2B. However, the EDS pattern indicates formation of cobalt metal particles with an FCC structure. Similarly, the XRD data indicate formation of cobalt metal particles after annealing (Figure 1) whereas, before, formation of Co_2B cannot be excluded. Segregation of Co_2B in Co_n under annealing can be excluded because (i) in the bulk phase, Co_2B is still stable at 500 K and no segregation occurs.[30] (ii) Co_2B nanoparticles, prepared in aqueous solution and having 2 nm average diameter, do not phase separate under annealing. The major effect is attributed to an increase in the particle size.[26]

Hence, the appearance of peaks due to cobalt metal (Figure 2B) can be attributed to an increase in the particle size and not to a phase separation taking place during annealing.

Furthermore, the magnetization data favor formation of cobalt metal nanoparticles. In fact, the anisotropy constant value, determined from the blocking temperature of the ZFC curve (Figure 4), is 2.4×10^6 erg/cm^3, whereas it is 2.7×10^6 erg/cm^3 for FCC cobalt metal in the bulk phase.[14] Also, it is very high compared to that of the Co_2B bulk phase (5×10^4 erg/cm^3).[30] However, it can be noticed that the anisotropy constant of nanoparticles is always higher than that of the bulk phase and decreases with increasing particle size (8, 10C, 14). The change in the anisotropy constant is always lower than a factor of 10. So we could expect that the anisotropy constant of Co_2B nanoparticles is lower than that of the Co_n bulk phase. Furthermore, the particle size (Figure 3) is rather high and the anisotropy constant does not markedly differ from the bulk phase. This confirms the observation that the bulk properties are rapidly reached when the number of cobalt atoms in the aggregates increases.[8] The SAXS data show formation of a sharp interface without any shell structure. From these data it can be concluded that cobalt metal particles are formed. The absorption atomic spectroscopy data are explained by assuming that the chemical reduction of $Co(AOT)_2$ by $NaBH_4$ in reverse micelles is similar to that described above in a homogeneous nonpolar solvent.[27] In this case, the surfactant acts as a ligand with formation of cobalt metal nanoparticles and B_2H_6 (eqs 3 and 4). All the borane, B_2H_6, formed is complexed during the various extraction steps, first with trioctylphosphine and then with pyridine, and it follows the extraction process. From the chemical reaction described in eqs 3 and 4, the relative ratio in weight of B/Co is 36.7 wt %. This value is very close to that determined by atomic absorption spectroscopy (37%). This allows us to conclude that reactions 3 and 4 take place and FCC cobalt metal particles are formed. Cobalt metal nanoparticles with a FCC structure have been observed for nanosized cobalt particles made in reverse micelles[14] and for graphite encapsulated 10 nm cobalt nanoparticles obtained by electrical arc techniques.[32] Cobalt FCC seems to be the stable phase at room temperature of the nanoparticles, whereas it is not in the bulk phase. Hence, from these data it can be concluded that chemical reduction of $Co(AOT)_2$ by $NaBH_4$ induces formation of FCC cobalt nanoparticles. However, we cannot exclude small inclusions of boron in the metal matrix.

The estimated saturation magnetization of particles dispersed in pyridine is low (80 emu/g) compared to that of the FCC bulk material (162 emu/g). This large discrepancy can be attributed

to the strong interactions between both pyridine and trioctylphosphine with cobalt atoms at particle surfaces. This behavior cannot be checked under our experimental conditions because the coated particles are not soluble in solvents other than pyridine. However, it was recently shown that species adsorbed on metal magnetic nanoparticles, especially electron donors such as pyridine, change the magnetization and "killed" the surface contribution.[31] This was calculated and observed for a small nickel cluster ($Ni_{38}Pt_6$) coated by CO ligands. These carbonyls completely quench the magnetic moments of the nickel atoms at the surface of the cluster, leaving the inner-core metal atoms unaffected. The smaller the particle size the greater is the surface contribution and thus the total decrease. Similar interactions between the species adsorbed at the surface of the cobalt nanoparticles could explain the decrease of the magnetization at saturation of coated cobalt nanoparticles dispersed in pyridine (Table 2).

Particles arranged in a 2D superlattice are obtained by evaporation of a solution containing particles dispersed in pyridine. The magnetization of the monolayers deposited on the graphite substrate shows a marked increase of M_r/M_s from 0.25 to 0.45 in comparison to the case of isolated nanoparticles (Table 2). Furthermore, saturation magnetization is reached at 1.5 T. However, this saturation magnetization is close to that obtained for particles dispersed in pyridine and still smaller than that of the bulk phase. This is because, even after evaporation, pyridine molecules remain bound to the interface with formation of strong complexes with cobalt atoms. Such changes in the magnetization between particles dispersed in pyridine and deposit on a support cannot be attributed to coalescence of the aggregates. This is clearly shown from the TEM pattern over a long distance. This change in magnetization is attributed to the collective flip of the magnetization of adjacent particles that could be explained by a change of the magnetization when nanoparticles are organized in 2D compared to a random distribution. This is confirmed by an increase in the blocking temperature when particles are arranged in 2D superlattices. Some attempt was made to model the magnetism of aggregates of nanoparticles and predict a collective effect producing a hysteresis loop at low temperature for identical spherical particles without anisotropy in dipolar interactions.[33]

V. Conclusion

We report the formation of cobalt nanosized particles in a 2D self-assembled hexagonal network. These particles are from an initial "in situ" synthesis in colloidal assemblies. Due to their small size the cobalt nanoparticles are in the FCC state, showing the anisotropy energy constant, K_a, of the FCC bulk cobalt. Passivation of the surface gives a marked decrease in the size distribution. This favors the formation of 2D superlattices of 5.8 nm diameter cobalt particles.

Comparison of the hysteresis loop at 3 K between the isolated particles dispersed in pyridine and particles in the self-assembled state shows a collective effect due to the 2D organization. This is, to our knowledge, the first signature of a collective effect in magnetization of 5.8 nm colloidal nanoparticles in a self-assembled hexagonal state.

Acknowledgment. The TEM experiments were performed at the CEA-Saclay DCC/DESD/SESD-Laboratoire de géochimie du Solide. We are most grateful to Dr. M. Julien for his hospitality and experimental help. Thanks are due also to Dr. J. Hommor, Dr. E. Vincent and Dr. G. Lebras, from CEA-Saclay/DRECAD/SPEC for their help in Magnetization Experiment.

References and Notes

(1) Special issue "Nanostructured Materials". *Chem. Mater.* **1996**, *8*, No. 5.

(2) Pileni, M. P. *J. Phys. Chem.* **1993**, *97*, 9661; *Langmuir*, **1997**, *13*, 3266.

(3) (a) Wang Y. *Acc. Chem. Res.* **1991**, *24*, 133 and reference therein. (b) Meisel, D. *Curr. Opinion Colloid Interface Sci.* **1997**, *2*, 188.

(4) (a) Petit C.; Pileni, M. P. *J. Phys. Chem.* **1988**, *92*, 228. (b) Cizeron, J.; Pileni, M. P. *J. Phys. Chem.* **1995**, *99*, 17410. (c) Alivisatos, A. P. *Science* **1996**, *271*, 933. (d) Levy L.; Hochepied J. F.; Pileni, M. P. *J. Phys. Chem.* **1996**, *100*, 18322. (e) Mulvaney, P. In *Semiconductor Nanocluster. Studies in Surface Science and Catalysis*; Kamat, P. V., Meisel, D., Eds.; Elsevier Science: Amsterdam, 1996; Vol. 103.

(5) (a) Petit, C.; Lixon, P.; Pileni, M. P. *J. Phys. Chem.* **1993**, *97*, 12974. (b) Lisiecki, I.; Pileni, M. P. *J. Am. Chem. Soc.* **1993**, *97*, 12974. (c) Hövel, H.; Fritz, S.; Hilger, A.; Kreibig, U.; Volker, M. *Phys. Rev. B* **1993**, *48*, 18178. (d) Alvarez, M. M.; Koury, J. T.; Schaaf, T. G.; Shafigullin, M. N.; Vezmar, I.; Whetten, R. L. *J. Phys. Chem. B* **1997**, *101*, 3706.

(6) For review, see: Awschalom, D. D.; DiVencenzo, D. P. *Phys. Today* **1995**, *48*, 43.

(7) Shi, J.; Gider, S.; Babcock, K.; Awschalom D. D. *Science* **1996**, *271*, 937.

(8) Billas, I.; Châtelain, A.; de Heer W. A. *J. Magn. Magn. Mater.* **1997**, *168*, 64.

(9) Eastoe, J.; Warne B. *Curr. Opinion Colloid Interface Sci.* **1996**, *1*, 800.

(10) (a) Moumen, N.; Veillet, P.; Pileni, M. P. *J. Magn. Magn. Mater.* **1995**, *149*, 67. (b) Moumen, N.; Bonville, P.; Pileni, M. P. *J. Phys. Chem.* **1996**, *100*, 14410. (c) Moumen, N.; Pileni, M. P. *J. Phys. Chem.* **1996**, *100*, 1867.

(11) Petit, C.; Pileni, M. P. *J. Magn. Magn. Mater.* **1997**, *166*, 82.

(12) Feltin, N.; Pileni, M. P. *Langmuir* **1997**, *13*, 3927.

(13) (a) Chen, J. M.; Lee, K. M.; Sorensen, C. M.; Klabunde, K. J.; Hadjipanayis G. C. *J. Appl. Phys.* **1994**, *76*, 5876 and 6316. (b) Ziolo, R. F.; Gianellis, E. P.; Weinsteins, B. A.; O'Horo, M. P.; Ganguly, B. N.; Mehrotra, V.; Russel, M. W.; Hoffman, D. R. *Science* **1992**, *257*, 219. (c) Mann, S.; Archibald, D. O.; Didymus, J. M.; Douglas, T.; Heywood, B. R.; Meldrum, F. C.; Reeves, N. J. *Science* **1993**, *261*, 1286.

(14) Chen, J. M.; Sorensen, C. M.; Klabunde, K. J.; Hadjipanayis, G. C. *Phys. Rev. B* **1995**, *51*, 11527.

(15) Taleb, A.; Petit, C.; Pileni, M. P. *Chem. Mater.* **1997**, *9*, 950.

(16) (a) Motte, L.; Billoudet, F.; Lacaze, E.; Douin, J.; Pileni, M. P. *J. Phys. Chem. B* **1997**, *101*, 138. (b) Motte, L.; Billoudet, F.; Pileni, M. P. *J. Phys. Chem.* **1995**, *99*, 16425.

(17) (a) Rousseaux, F.; Chen, Y.; Haghiri, A. M.; Launois, H. *Nucl. Instrum. Methods Phys. Res.* **1995**, *A359*, 388. (b) Hehn, M.; Ounadjela, K.; Bucher, J. P.; Rousseaux, F.; Decanini, D.; Bartenlian, B.; Chappert, C. *Science* **1996**, *272*, 1782.

(18) Fettar, F.; Petroff, F.; Maurice, J. L.; Vaurès, A.; Schelp, L. F.; Fert, A. Babonneau, D.; Naudon, A. In *Books of the Abstracts of the 5th Colloque Louis Néeel*; France, 1997.

(19) Yin, J. S.; Wang, Z. L. *J. Phys. Chem. B* **1997**, *101*, 8979.

(20) Yin, J. S.; Wang, Z. L. *Phys. Rev. Lett.* **1997**, *79*, 2570.

(21) (a) Guinier, A.; Fournet, G. *Small Angle Scatterings of X-rays*; Wiley: New York, 1955. (b) Glatter, O. Small Angle Scattering and Light Scattering. In *Neutron, X-ray and Light Scattering: Introduction to an Investigate Tool for Colloidal and Polymeric Systems*; Lindner, P., Zemb, T., Eds.; North-Holland Delta Series: Amsterdam, 1991.

(22) Porod, G. In *Small angle X-ray Scattering;* Glatter, O., Kratky, O., Eds.; Academic Press: New York, 1982; Chapter 2.

(23) Petit, C.; Taleb, A.; Pileni, M. P. *Adv. Mater.* **1998**, *10*, 259.

(24) JCPDS, *international centre for diffraction data*, file No 15-806.

(25) Glavee, G. N.; Klabunde, K. J.; Sorensen, C. M.; Hadjipanayis, G. C. *Langmuir* **1993**, *9*, 162.

(26) Glavee, G. N.; Klabunde, K. J.; Sorensen, C. M.; Hadjipanayis, G. C. *Langmuir* **1994**, *10*, 4726.

(27) Glavee, G. N.; Klabunde, K. J.; Sorensen, C. M.; Hadjipanayis, G. C. *Inorg. Chem.* **1993**, *32*, 474.

(28) Onori, G.; Santucci, A. *J. Phys. Chem.* **1994**, *57*, 5430.

(29) *Comprehensive Inorganic Chemistry*; Trotman-Dickerson, A. F., Ed.; Pergamon Press: Oxford, U.K., 1973.

(30) *Landolt Bornstein*; Bertotti, G.; Ferchmin, A. R.; Madelong, O., Eds.; News Series III, Vol. 19b; Springer: Berlin, 1994, p 244.

(31) van Leeuwen, D. A.; van Ruitenbek, J. M.; de Jongh, L. J.; Ceriotti, A.; Pacchioni, G.; Häberlen, O. D.; Rösch N. *Phys. Rev. Lett.* **1994**, *73*, 1432.

(32) Host, J. J.; Block, J. A.; Parvin, K.; Dravid, V. P.; Alpers, J. L.; Sezen, T.; LaDuca, R. *J. Appl. Phys.* **1998**, *83*, 793.

(33) Ferré, R.; Barabara, B. In *Books of the Abstracts of the 5th Colloque Louis Néeel*; France, 1997.